In Vivo Uptake of Polyisobutyl Cyanoacrylate Nanoparticles by Rat Liver Kupffer, Endothelial, and Parenchymal Cells

V. LENAERTS *, J. F. NAGELKERKE ‡, T. J. C. VAN BERKEL ‡, P. COUVREUR *x, L. GRISLAIN *, M. ROLAND *, and P. SPEISER §

Received November 10, 1982, from the *Laboratoire de Pharmacie Galénique, Université Catholique de Louvain, B-1200 Brussels, Belgium, the ‡Department Biochemistry 1, Erasmus University, 3000-DR Rotterdam, The Netherlands, and the §School of Pharmacy, Federal Institute of Technology, Zürich, Switzerland. Accepted for publication June 23, 1983.

Abstract □ Polyalkyl cyanoacrylate nanoparticles were previously developed as a biodegradable, ultrafine, solid drug carrier. Distribution studies in the rat showed an intense and rapid hepatic uptake. This liver accumulation appears to represent, to a certain extent, extracellularly bound nanoparticles. During liver perfusion, 15–20% of the liver-associated nanoparticles were washed out. The cellular distribution of strongly cell-associated nanoparticles was determined. At different intervals after injection of radioactive nanoparticles to rats, the cells were isolated according to a recently developed, low-temperature procedure during which processing of the carrier was inhibited. At all tested times, a relatively intense capture by Kupffer cells in comparison with endothelial and especially parenchymal cells was observed. This distribution pattern was not influenced by the size of the nanoparticles (0.08–0.215-μm diameter). This specific interaction of nanoparticles with Kupffer cells opens possibilities for the treatment of some parasitic diseases involving this cell type.

Keyphrases □ Nanoparticles—polyisobutyl cyanoacrylate, *in vivo* uptake, rat liver Kupffer, endothelial, and parenchymal cells □ Polyisobutyl cyanoacrylate—*in vivo* uptake of nanoparticles, rat liver Kupffer, endothelial, and parenchymal cells □ Distribution—*in vivo* uptake of polyisobutyl cyanoacrylate nanoparticles, rat liver Kupffer, endothelial, and parenchymal cells

The incorporation of a drug into a carrier such as liposomes, macromolecules, or solid colloidal nanoparticles modifies the body distribution of the drug (1–3). This change in the distribution pattern can be used to direct a drug specifically to the target tissue or to protect a tissue from the toxic effects of a drug. For this purpose a carrier consisting of polyalkyl cyanoacrylate nanoparticles was developed (4, 5). These submicroscopic spheres, <0.3 μm in diameter, are degraded under physiological conditions (6, 7). Associated with a cytostatic drug, they provoke an enhancement of the therapeutic activity (8) or a reduction of the toxicity (9). The body distribution of these carriers was studied, and, as for most carriers, an intense and rapid capture by the organs rich in reticuloendothelial cells was observed (10, 11).

Since the majority of nanoparticles were captured by the liver, the intrahepatic distribution of the carriers as a function of time is important. Whether the interaction between nanoparticles and parenchymal cells could be affected by administration of nanoparticles smaller than the fenestrated lining of the liver sinusoids (0.1 μm) was studied.

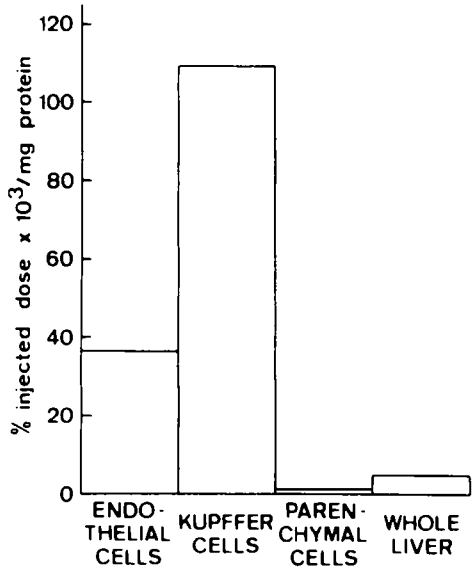

Figure 1—*Distribution of [^{14}C]polyisobutyl cyanoacrylate nanoparticles (0.215-μm diameter) in the rat liver Kupffer, endothelial, and parenchymal cells 30 min after intravenous administration.*

EXPERIMENTAL SECTION

Preparation of Radioactive Nanoparticles—Radioactive monomer was prepared according to a previously published method (12). [^{14}C]Formaldehyde was used in the synthesis; as a result, the monomer was tagged on the C-3 atom. The specific activity of the radioactive monomer[1] was 1.4 mCi/mL.

To a 10-mL solution of 1% dextran 70 and 0.05 M H_3PO_4 was added 0.1 mL of the radioactive monomer, with stirring. After 2 h of polymerization, the suspension was made isotonic with glucose and neutralized with 0.5 M NaOH. Smaller nanoparticles were prepared in a similar way, except the polymerization medium was a 5% glucose in 10^{-5} M HCl solution. The nanoparticles size was measured using a particle counter[2], based on laser beam scattering.

Isolation and Separation of Rat Liver Parenchymal, Kupffer, and Endothelial Cells—After intravenous administration of radioactive nanoparticles to rats (Wistar R1)[3], at different intervals, cell isolation was started by a liver perfusion, first with Ca^{2+}-free Hank's buffer at 8°C and then with 1 mM $CaCl_2$ Hank's buffer at 8°C containing either 0.5% (w/v) collagenase[4] for parenchymal cell isolation or 0.25% protease[5] for Kupffer and endothelial cell isolation. Further isolation was performed at 0°C to minimize degradation and redistribution of the internalized nanoparticles. Further purification of the Kupffer and endothelial cells was performed according to a modified version of a published method (13), which is described in detail elsewhere together with the parenchymal cells isolation technique (14). Kupffer and endothelial cells were obtained by, successively, 400×*g* centrifugation, metrizamide[6] density cushion centrifugation, and centrifugal elutriation[7].

The absence of parenchymal cell remnants was indicated by the absence of L-type pyruvate kinase (15, 16). The characterization of Kupffer and endothelial cell preparations was realized by light microscopic examination after staining for peroxidase activity with diaminobenzaldehyde (17) followed by a Papanicolaou counter-staining (18). After this treatment Kupffer cells were easily recognized by their brown appearance, while endothelial cells were blue. The purity of the endothelial cells preparations was >95%, while the purity of the Kupffer cells preparations was between 70 and 90%, the remainder being endothelial cells.

[1] I.R.E., Fleurus, Belgium.
[2] Nanosizer; Coulter Co. Ltd., Harpenden, England.
[3] C.P.B.; Erasmus University, Rotterdam, The Netherlands.
[4] 200 U/mg, type I; Sigma, St. Louis, Mo.
[5] Pronase, 50,000 PUK/mg, B-grade; Calbiochem-Behring, La Jolla, Calif.
[6] Metrizamide; Nyegaard and Co., A-S, Oslo, Norway.
[7] Beckman Elutriaton Rotor System; Beckman Instruments, Palo Alto, Calif.

0022-3549/84/0700-0980$01.00/0

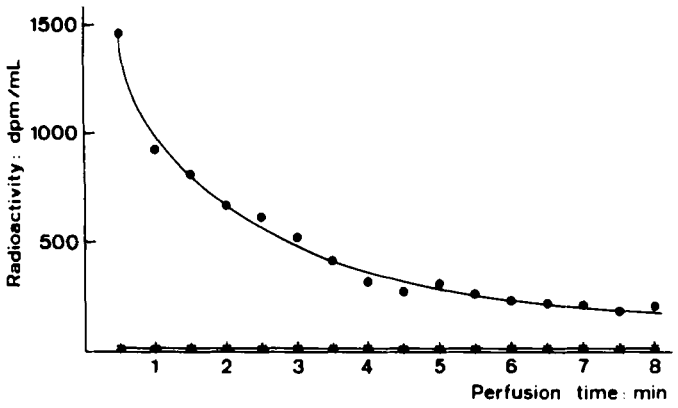

Figure 2—*Radioactivity present in fractions of the liquid collected from the rat liver during a perfusion with Hank's medium at 8°C started 30 min after intravenous administration of [^{14}C]polyisobutyl cyanoacrylate nanoparticles. Radioactivity was measured in the pellets (*) and supernatants (●) of the fractions after a 5-min centrifugation at 600×g.*

Parenchymal cells were isolated by repeated low-speed centrifugations, essentially in the same way as reported previously (19). The parenchymal cell preparations were free of other cell types, as checked by light microscopy.

The total liver value was calculated from the radioactivity present in a liver lobe which was tied off after an 8-min perfusion with Ca^{2+}-free Hank's buffer, just prior to perfusion with proteolytic enzymes. The liver lobe, isolated cells, and samples of the nanoparticle preparation were oxidized[8] and radioactivity was counted by liquid scintillation[9]. The protein content in the samples was determined according to the method of Lowry (20), using bovine serum albumin[10] as a standard.

To determine the amount of loosely bound nanoparticles, radioactivity was measured in the postperfusion medium during an 8-min perfusion with Hank's Ca^{2+}-free medium at 8°C. This perfusion was started 30 min after the injection of nanoparticles and just after a liver lobe had been tied-off and excised to serve as a nonperfusion control. Furthermore, the different samples were centrifuged at 600×*g* for 5 min to check whether the radioactivity was due to nonsediment nanoparticles or to nanoparticle-carrying cells. All these samples were then counted for radioactivity.

RESULTS AND DISCUSSION

Intrahepatic Distribution of Nanoparticles—Figure 1 shows the distribution of the 0.215-nm ^{14}C-labeled polyisobutyl cyanoacrylate nanoparticles between the different liver cell types 30 min after intravenous administration. Nanoparticles were recovered mainly in the Kupffer cells. The association of nanoparticles to Kupffer cells (expressed per milligram of cell protein) was

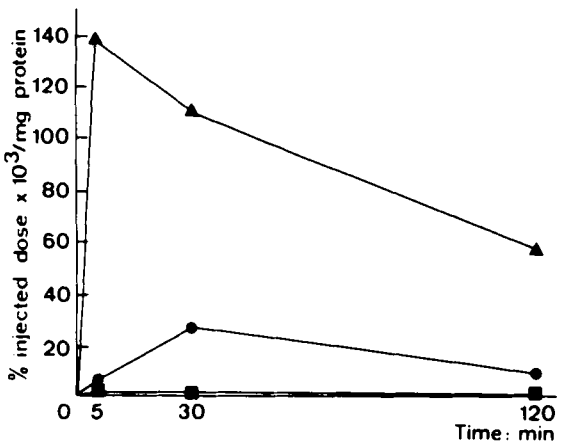

Figure 3—*Distribution of [^{14}C]polyisobutyl cyanoacrylate nanoparticles (0.215-μm diameter) in the Kupffer (▲), endothelial (●), and parenchymal (■) cells of a rat liver as a function of time after intravenous administration.*

[8] Packard Tri-Carb Oxidizer; Packard, Downers Grove, Ill.

[9] Packard Tri-Carb Liquid Scintillation Spectrometer; Packard, Downers Grove, Ill.

[10] Fraction V; Sigma, St. Louis, Mo.

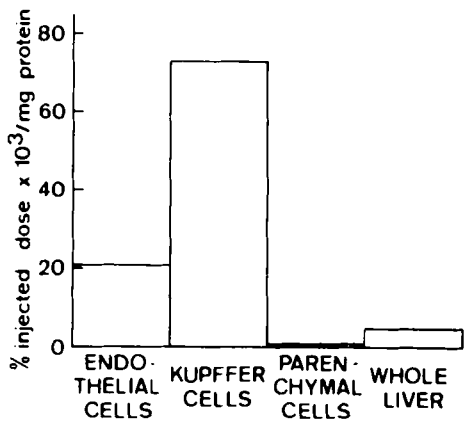

Figure 4—*Distribution of [^{14}C]polyisobutyl cyanoacrylate nanoparticles (0.08-μm diameter) in the rat liver Kupffer, endothelial, and parenchymal cells 30 min after intravenous administration.*

100-fold higher than with the major liver cell type (parenchymal cells). An intermediate cell accumulation value was observed for endothelial cell preparations.

Based on the relative contribution of Kupffer, endothelial, and parenchymal cells to total liver, the recovery of the radioactivity in the isolated cells as compared with that originally present in the whole liver can be calculated. This calculation indicates that the nanoparticles, present in the liver just before the perfusion with proteolytic enzymes, were quantitatively recovered in the isolated cells. This high recovery is only possible if the nanoparticles were either internalized or strongly associated with the liver cells. However, it was observed that during the Ca^{2+}-free perfusion, the loosely bound nanoparticles were removed (15–20% of the initial liver-associated radioactivity).

The total rat liver accumulation of radioactivity after an 8-min perfusion at 8°C was 13% of the injected dose. This value is somewhat lower than for the nonperfused liver (17% of the injected dose). This difference can only be explained by the release of loosely bound nanoparticles. Indeed, when the postperfusion medium was centrifuged at 600×*g* for 5 min, practically all radioactivity was found in the supernatant (Fig. 2). This result excludes the hypothesis of radioactive nanoparticle-containing cell release during the perfusion.

Liver Distribution as a Function of Time—Figure 3 shows the time course of the accumulation of nanoparticles into the different rat liver cell types. The association to Kupffer cells occurs very rapidly, while the maximal association to endothelial cells is clearly slower. However, at all time intervals tested, nanoparticles were always recovered mainly in the Kupffer cells. The radioactivity ratios of Kupffer to parenchymal cells were 173, 101, and 119, respectively, for intervals of 5, 30, and 120 min. For the same intervals, the ratios of Kupffer to endothelial cells were 21.2, 4.9, and 5.9.

Influence of Nanoparticle Size on Liver Distribution—The endothelial lining of the rat liver sinusoid contains fenestrae arranged in "sieve plates;" the pores of the fenestrae are ~0.1 μm in diameter (21). It can be argued that the low *in vivo* uptake of nanoparticles by the parenchymal cells is caused by this morphological barrier. If this is true, a drop in the particle size would enable an interaction with the parenchymal cells. For this purpose, the cellular distribution of particles with a mean diameter of 0.08 μm was studied 30 min after intravenous administration (Fig. 4). The uptake ratios of Kupffer to parenchymal cells and of Kupffer to endothelial cells were 92 and 3.6 for the 0.08-μm particles as compared with 101 and 4.2 for the 0.215-μm particles. These data indicate clearly that the interaction of nanoparticles with the different liver cells is not influenced by the size difference of the carrier.

CONCLUSIONS

After intravenous administration to rats, nanoparticles are localized in various compartments inside the liver. The data show that Kupffer cells are the major liver site for cell accumulation of the nanoparticles. This specific interaction is independent of the particle size in the range studied (0.08–0.215-μ diameter). Endothelial and especially parenchymal cells show a very low cell association with the nanoparticles. It is important to note that part of the nanoparticles remain loosely attached to the cells and can be released from their site by perfusion.

The interaction of nanoparticles with Kupffer cells should lead to specific drug delivery from this colloidal carrier. For the treatment of Kupffer cell-associated diseases, use of nanoparticles could be significant in achieving appropriate drug targeting.

REFERENCES

(1) G. Gregoriadis, E. Wills, C. Swain, and A. Tavill, *Lancet*, **i**, 1313 (1974).

(2) A. Trouet, D. Deprez-Decampeneere, M. Desmedt-Malengraux, and G. Atassi, *Eur. J. Cancer*, **10**, 405 (1974).

(3) P. Speiser, *Progr. Polym. Sci.*, **59**, 48 (1976).

(4) P. Couvreur, M. Roland, and P. Speiser, U.S. Patent 4,329,332 (1982).

(5) P. Couvreur, B. Kante, M. Roland, P. Guiot, P. Baudhuin, and P. Speiser, *J. Pharm. Pharmacol.*, **31**, 331 (1979).

(6) P. Couvreur, B. Kante, M. Roland, and P. Speiser, *J. Pharm. Sci.*, **68**, 1521 (1979).

(7) W. Vezin and A. Florence, *J. Biomed. Mat. Res.*, **14**, 93 (1980).

(8) F. Brasseur, P. Couvreur, B. Kante, L. Deckers-Passau, M. Roland, and C. Deckers, *Eur. J. Cancer*, **16**, 1441 (1980).

(9) P. Couvreur, B. Kante, L. Grislain, M. Roland, and P. Speiser, *J. Pharm. Sci.*, **71**, 790 (1982).

(10) B. Kante, P. Couvreur, V. Lenaerts, P. Guiot, M. Roland, P. Baudhuin, and P. Speiser, *Int. J. Pharm.*, **7**, 45 (1980).

(11) P. Couvreur, B. Kante, V. Lenaerts, V. Scailteur, M. Roland, and P. Speiser, *J. Pharm. Sci.*, **69**, 199 (1980).

(12) C. McKeever, U.S. Patent 2,912,454 (1959).

(13) D. P. Praaning-Van Dalen and D. L. Knook, *FEBS Letts.*, **141**, 2, (1982).

(14) J. F. Nagelkerke, K. P. Barto, T. J. C. Van Berkel, in "Sinusoidal Liver Cells," D. L. Knook and E. Wisse, Eds., Elsevier North-Holland Biomedical, Amsterdam, The Netherlands, 1983, pp. 319–326.

(15) T. J. C. Van Berkel, *Biochem. Biophys. Res. Comm.*, **61**, 204 (1974).

(16) J. F. Nagelkerke, K. P. Barto, T. J. C. Van Berkel, *Exp. Cell. Res.*, **138**, 183 (1982).

(17) H. D. Fahimi, *J. Cell Biol.* **47**, 247 (1970).

(18) L. G. Koss, in "Diagnostic Cytology," 3rd ed., Lippincott, Philadelphia, Pa. 1979, 1211–1222.

(19) M. N. Berry and D. S. Friend, *J. Cell Biol.*, **43**, 506 (1969).

(20) K. H. Lowry, N. J. Rosebrough, A. L. Farr, and R. J. Randall, *J. Biol. Chem.*, **193**, 265 (1951).

(21) E. Wisse in "Kupffer Cells and Other Sinusoidal Cells," E. Wisse and D. L. Knook, Eds., Elsevier North-Holland Biomedical Press, Amsterdam, The Netherlands, 1977, pp. 33–60.

ACKNOWLEDGMENTS

J.F.N. is supported by Grant 13-53-07 from the Foundation of Fundamental Medical Research (FUN 60). This work was supported by the Sopar S.A. Co. and by the Institut pour l'Encouragement de la Recherche Scientifique dans l'Industrie et l'Agriculture (I.R.S.I.A.). The kind support of the Assurances Générales de France was greatly appreciated.

The authors are thankful to Mr. Barto and Mrs. Duhamel for skillful assistance, to Mr. Vandiest for the drawings and the photographic work, and to Mrs. D'Heur for secretarial work.

Synthesis and Antimicrobial Activity of Novel Quinazolone Derivatives

N. S. HABIB * and M. A. KHALIL ‡x

Received February 14, 1983, from the **Pharmaceutical Chemistry Department, Faculty of Pharmacy, University of Alexandria, Egypt* and the ‡*College of Pharmacy, Florida A&M University, Tallahassee, FL 32307.* Accepted for publication May 11, 1983.

Abstract □ Three novel series of 4-oxoquinazoline derivatives were prepared and evaluated as potential antimicrobial agents. Evaluation of the antimicrobial activity of a variety of 4-substituted-1-thiosemicarbazides, 3,4-disubstituted thiazolines, and 3-substituted-5-thiazolidones reveals that the majority possess significant *in vitro* activity against Gram-positive organisms. Some derivatives also exhibited antifungal activity.

Keyphrases □ 4-Oxoquinazoline analogues—synthesis, antimicrobial activity, *in vitro* screen □ Antimicrobial agents—potential, 4-oxoquinazoline analogues, synthesis

There has been considerable interest in various 4-oxoquinazoline analogues. Some have shown a wide spectrum of biological effects (1–5) including antitubercular (6), antibacterial (7), and antifungal (8) activities. Thiazoline analogues were also reported to exhibit antitubercular (9) and antibacterial (10) activities. These observations prompted us to synthesize a variety of compounds containing the thiazoline nucleus and examine them for antimicrobial activity (11). Recently, the antimicrobial activities of some 4-oxoquinazoline thiosemicarbazides and thiazoline derivatives were investigated (12).

In a continuing effort to develop new antimicrobial agents, 1- [4- (2-methyl-4-oxoquinazoline-3-yl)benzoyl] -4-alkyl-, -aryl-, and -aralkyl-3-thiosemicarbazides (VII–X), 3,4-disubstituted thiazoline-2-oxo[4-(2-methyl-4-oxoquinazoline-3-yl)benzoyl]hydrazones (XI–XIV), and 3-substituted 5-thiazolidone-2-oxo-[4-(2-methyl-4-oxoquinazoline-3-yl)-benzoyl]hydrazones (XV–XVIII) were synthesized and evaluated as potential antimicrobial agents.

RESULTS AND DISCUSSION

Chemistry—Treatment of 2-substituted-4-oxoquinazolines, with hydrazine hydrate results in hydrazinolysis of the quinazolone ring to give 3-amino-2-substituted-4-oxoquinazolines (13). In the present investigation, as shown in Scheme I, heating 3-(4-carbethoxyphenyl)-2-methyl-4-oxoquinazolone (I) with hydrazine hydrate resulted in the formation of three products: *p*-aminobenzoic acid hydrazide (II), 4-(2-methyl-4-oxoquinazoline-3-yl)benzoic acid hydrazide (III) (as a minor product), and 3-amino-2-methyl-4-oxoquinazoline (IV). Compounds II and IV were identified by TLC, IR, and mixed melting point comparisons with authentic samples prepared by the previously reported methods (14, 15), while III was identified by IR spectrometry and elemental analysis. The formation of these three different products might indicate that hydrazine attacks first the ester side chain of I, then the quinazolone nucleus. This appears to be true since the treatment of III with hydrazine, resulted in the formation of II and IV. More evidence was obtained when we found that the hydrazine hydrate can replace substituted hydrazine from the quinazolone nucleus. This was shown by the hydrazinolysis of 3-(4-carbethoxyphenylamino)-2-methyl-4-oxoquinazoline (V) into IV and *p*-hydrazinobenzoic acid hydrazide (VI) (Scheme I).

In the present work, the intermediate 4-(2-methyl-4-oxoquinazoline-3-yl)benzoic acid hydrazide (III) was prepared in a higher yield, under carefully controlled reaction conditions by treating hydrazine hydrate with I at room temperature for 1 h. As outlined in Scheme II, treatment of III with the selected alkyl-, aryl-, or aralkylisothiocyanate in refluxing ethanol afforded the desired thiosemicarbazides (VII–X) (Table I). Reaction of the formed thiosemicarbazides with phenacyl bromide or ethyl bromoacetate gave the thiazoline (XI–XIV) or thiazolidone (XV–XVIII) derivatives, as shown in Table II and Table III, respectively. The products were identified by elemental

0022-3549/84/0700-0982$01.00/0